



Short communication

High performance air electrode for solid oxide regenerative fuel cells fabricated by infiltration of nano-catalysts



Sung-il Lee^a, Jeonghee Kim^{a,b}, Ji-Won Son^a, Jong-Ho Lee^a, Byung-Kook Kim^a,
Hae-June Je^a, Hae-Weon Lee^a, Huesup Song^c, Kyung Joong Yoon^{a,*}

^a High-Temperature Energy Materials Research Center, Korea Institute of Science and Technology, Hwarangno 14-gil 5, Seongbuk-gu, Seoul 136-791, Republic of Korea

^b Department of Fuel Cells and Hydrogen Technology, Hanyang University, Seoul, Republic of Korea

^c Division of Advanced Materials Engineering, Kongju National University, Chonan, Republic of Korea

HIGHLIGHTS

- High performance air electrode is fabricated by nano-catalyst infiltration.
- Homogeneous nano-catalysts are formed by urea decomposition.
- Surface chemical exchange is accelerated by nano-catalysts.
- Performance is improved for power generation and hydrogen production.
- Nano-catalysts are stable against coarsening at high temperatures.

ARTICLE INFO

Article history:

Received 3 September 2013

Received in revised form

25 October 2013

Accepted 25 October 2013

Available online 6 November 2013

Keywords:

Nano-catalyst

Air electrode

Solid oxide fuel cell

Solid oxide electrolysis cell

Solid oxide regenerative fuel cell

ABSTRACT

A high performance air electrode fabricated by infiltration of highly active nano-catalysts into a porous scaffold is demonstrated for high-temperature solid oxide regenerative fuel cells (SORFCs). The nitrate precursor solution for $\text{Sm}_{0.5}\text{Sr}_{0.5}\text{CoO}_3$ (SSC) catalyst is impregnated into a porous $\text{La}_{0.6}\text{Sr}_{0.4}\text{Co}_{0.2}\text{Fe}_{0.8}\text{O}_3$ (LSCF)–gadolinia-doped ceria (GDC) composite backbone, and extremely fine SSC nano-particles are uniformly synthesized by *in-situ* crystallization at the initial stage of SORFC operation via homogeneous nucleation induced by urea decomposition. The SSC nano-catalysts are in the size range of 40–80 nm and stable against coarsening upon the SORFC operation at 750 °C. The electrochemical performance is significantly improved by incorporation of SSC nano-catalysts in both power generation and hydrogen production modes. Systematic analysis on the impedance spectra reveals that the surface modification of the air electrode with nano-catalysts remarkably accelerates the chemical surface exchange reactions for both O_2 reduction and O^{2-} oxidation, which are the major limiting processes for SORFC performance.

© 2013 Elsevier B.V. All rights reserved.

1. Introduction

In recent years, solid oxide regenerative fuel cell (SORFC) technology has attracted increasing attention for development of a highly-efficient energy conversion and storage system because a single SORFC unit can perform the dual functions of a solid oxide fuel cell (SOFC) and solid oxide electrolysis cell (SOEC) [1,2]. Although the overall SOEC reaction for hydrogen production is simply the reverse of the SOFC reaction for power generation, there are fundamental differences in two operating modes, such as the

mass flux, heat flow, electric potential and gas environments, which strongly influence the performance and system efficiency. It is generally accepted that the performance of an SOEC is inferior to that of an SOFC [3], and in particular, the polarization loss occurring at the air electrode dominates the overall performance [4]. It was reported that the surface chemical exchange is the major rate limiting process for the conventional mixed ionic-electronic conducting (MIEC) air electrodes [5], which emphasizes the need of improved electrode materials and/or structures with enhanced electrocatalytic activity toward O_2 reduction and O^{2-} oxidation for a successful development of SORFC technology. Although extensive research efforts have been devoted to reduction of the polarization loss of the air electrode, satisfactory materials and structures for SORFC still remain elusive.

* Corresponding author. Tel.: +82 2 958 5515; fax: +82 2 958 5529.

E-mail addresses: kyungjoong.yoon@gmail.com, kjyoon@kist.re.kr (K.J. Yoon).

Among the number of advanced electrode materials proposed to date, $\text{Sm}_{0.5}\text{Sr}_{0.5}\text{CoO}_3$ (SSC) exhibits an excellent surface oxygen exchange rate, electrical conductivity and bulk oxygen ion diffusion coefficient [6–8]. However, its practical application as a porous electrode has been limited due to the lack of the thermal compatibility and high cost; i.e., the large thermal expansion coefficient of SSC ($20 \times 10^{-6} \text{ K}^{-1}$) makes it extremely difficult to secure a stable interface with other cell components in a multi-layer structure during fabrication, operation, and thermal cycles [9,10], and the use of samarium in large scale is undesirable due to its high cost [11]. These technical challenges can be overcome and the merits of SSC can be efficiently utilized by incorporating a small amount of SSC catalyst into the stable porous scaffold in the form of nano-particles. As it is extremely difficult to infiltrate and uniformly distribute the pre-synthesized nano-particles inside the porous scaffold with submicron-scale pores, it is preferable to inject a precursor solution into the pores and then thermally treat to form the desired phase through precipitation and decomposition of metal salts. In typical solution impregnation techniques, the concentration of nano-particles is higher near the exposed surface because the precipitation of metal salts is induced by drying process [12]. Such segregation may disrupt the effectiveness of nano-catalyst incorporation because the electrochemical reaction predominantly occurs near the electrode-electrolyte interface. In this work, advanced infiltration and *in-situ* crystallization technique, where precipitation occurs via homogeneous nucleation induced by urea decomposition, was developed to obtain uniform distribution of SSC nano-catalysts throughout the porous $\text{La}_{0.6}\text{Sr}_{0.4}\text{Co}_{0.2}\text{Fe}_{0.8}\text{O}_3$ (LSCF)–gadolinia-doped ceria (GDC) composite air electrode. The phase formation, morphology and distribution of nano-catalysts were investigated in the urea decomposition technique. The electrochemical performance and stability were evaluated in SOFC operation, and the effect of nano-catalyst incorporation on the electrode reaction kinetics and overall performance of SOFC was discussed in detail.

2. Experimental

For fabrication of hydrogen electrode substrate, NiO, yttria-stabilized zirconia (YSZ), and a poly(methyl methacrylate) (PMMA) pore-forming agent were mixed via ball-milling for 24 h in ethanol with a dispersant, binder and plasticizer, and granules were obtained by spray drying. A NiO, YSZ, and PMMA volume ratio was 0.37:0.33:0.3. The substrates (2 cm × 2 cm) were fabricated by the uni-axial pressing of the granules at 60 MPa. The slurries for the hydrogen electrode functional layer (NiO/YSZ), electrolyte (YSZ), interdiffusion barrier layer (GDC), air electrode functional layer (LSCF + GDC), and air electrode current-collecting layer (LSCF) were prepared by mixing ceramic powders with a dispersant, binder, and plasticizer in α -terpineol using a planetary mill for the subsequent screen-printing. The hydrogen electrode functional layer and electrolyte were screen printed sequentially, followed by co-sintering at 1370 °C. The GDC interdiffusion barrier layer was screen-printed on top of the co-sintered YSZ electrolyte and fired at 1250 °C. Next, the LSCF–GDC air electrode functional layer and LSCF current-collecting layer were screen-printed and sintered at 1050 °C in air. The effective electrode area was 1 cm × 1 cm. Details on the cell fabrication procedure is described in our previous publication [13].

A 1 mol L⁻¹ SSC precursor solution was prepared by mixing $\text{Sm}(\text{NO}_3)_3 \cdot 6\text{H}_2\text{O}$, $\text{Sr}(\text{NO}_3)_2$, $\text{Co}(\text{NO}_3)_2 \cdot 6\text{H}_2\text{O}$ and urea in a solvent composed of water and ethanol. The [urea]/[cation] ratio was 10, and the [water]/[ethanol] volume ratio of the solvent was 1.7. Infiltration was performed using a micro-syringe, followed by thermal treatment at 80 °C for 2 h. The infiltration and thermal

treatment steps were repeated 3 times before *in-situ* crystallization at 800 °C in cell operation. In a separate experiment, the crystallization behavior of SSC and its chemical compatibility with LSCF was investigated by dispersing LSCF powder in the SSC precursor solution, thermally treating it at 80 °C for 2 h and 800 °C for 72 h, and examining the crystal structure of the resulting powder using X-ray diffraction (XRD).

The cells were tested with humidified H₂ containing 3–50% H₂O on the hydrogen electrode and air on the air electrode between 700 and 800 °C for both power generation and hydrogen production modes. The gas flow rates were fixed at 200 sccm for both electrodes. Electrochemical characterization was performed using a Solartron 1260/1287 frequency response analyzer and potentiostat. Current collection was made using Pt mesh on the air electrode and Ni foam on the fuel electrode. No current collection paste was used. After testing, the cells were sectioned and parts of the cells were impregnated with epoxy in a vacuum. After the epoxy had hardened, the samples were polished down to 0.25 μm. The cross-sections of the fractured and polished surfaces were examined using scanning electron microscopy (SEM).

3. Results and discussion

In infiltration process for synthesizing the ceramic nano-catalysts, the processing temperature required for formation of the desired crystal structure plays a critical role in the size and morphology of the nano-particles. In SOFC applications, it is desirable to crystallize the nano-catalysts at the temperatures not substantially higher than the operating temperature because it enables the simple *in-situ* crystallization process during operation and prevents the excessive particle growth and unwanted chemical interactions. In Fig. 1, the phase formation of SSC nano-catalysts and their chemical compatibility with LSCF backbone are examined at 800 °C via XRD analysis. In this experiment, pre-synthesized LSCF powder was dispersed in the chemical solution containing SSC nitrate precursors and urea, with a [urea]/[cation] ratio of 10. Then, urea decomposition was performed at 80 °C, followed by calcination at 800 °C in air. The phase purity of the resulting SSC–LSCF composite powder was examined by XRD. All of the major peaks in the XRD pattern in Fig. 1 are identified as the SSC and LSCF perovskite structures, and secondary phase formation is not detected within the instrument sensitivity. In the urea

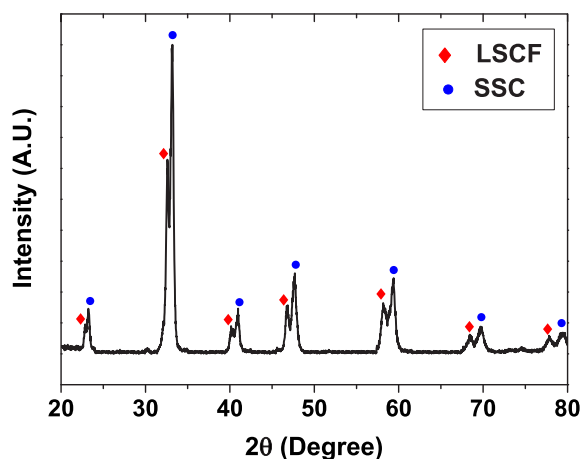


Fig. 1. XRD pattern of the SSC–LSCF powder mixture, showing the crystallization behavior of SSC derived from the precursor solution and its chemical compatibility with LSCF at 800 °C. The powder mixture was prepared by dispersing LSCF powder in the SSC precursor solution and thermally treating it at 80 °C for 2 h and 800 °C for 72 h in air.

decomposition process, crystallization behavior is strongly influenced by the [urea]/[cation] ratio because urea serves as a complexing agent as well as a precipitation agent [14]. Specifically, urea complexes with metal cations upon mixing and decomposes upon heating to $\sim 80^\circ\text{C}$, leading to the slow and controlled release of ammonia and carbon dioxide into the solution [15]:



As a consequence, the pH of the solution continuously increases, and the steady supply of OH^- and CO_3^{2-} ions induces the precipitation of metal hydroxides and hydroxycarbonates, which act as the precursors for the formation of the desired ceramic phase in the subsequent calcinations process. The absence of the un-reacted phases in Fig. 1 confirms the complete phase formation of perovskite SSC, which suggests that a [urea]/[cation] ratio of 10 is sufficient for crystallization at 800°C . In addition, no additional reaction products or major peak shifts are observed due to the chemical interaction with LSCF, which indicates that the SSC nano-catalysts and LSCF backbone are chemically compatible at the processing and operating temperatures. Therefore, the results in Fig. 1 imply that *in-situ* crystallization is viable for the formation of the SSC nano-catalysts at the early stage of the SORFC operation, which simplifies the fabrication process and avoids the coarsening of the nano-particles due to the exposure to excessively high temperatures.

The microstructure of the SORFC used in this study is displayed in Fig. 2(a). The cell is composed of a porous Ni–YSZ hydrogen electrode substrate ($\sim 800\ \mu\text{m}$), a fine and porous Ni–YSZ hydrogen electrode functional layer ($\sim 7\ \mu\text{m}$), a dense YSZ electrolyte ($\sim 6\ \mu\text{m}$), a partially dense GDC interdiffusion barrier layer ($\sim 6\ \mu\text{m}$), a fine and porous LSCF–GDC air electrode functional layer ($\sim 12\ \mu\text{m}$), and a porous LSCF air electrode current collecting layer ($\sim 16\ \mu\text{m}$). The backscattered electron image of the LSCF–GDC composite air electrode in Fig. 2(b) discriminates two separate phases, and energy dispersive spectroscopic analysis reveals that the LSCF is gray and the GDC is white. Two phases are mixed homogeneously in a very fine scale with the average particle diameter of $\sim 0.4\ \mu\text{m}$ for both LSCF and GDC. The volume fraction of pores and average pore diameter are $\sim 28\%$ and $\sim 0.7\ \mu\text{m}$, respectively, based on the image analysis. Whereas such fine microstructure of the air electrode is beneficial for increasing the active area available for the electrochemical reactions, the challenge arises in impregnating the solution into the submicron-scale pores, which emphasizes the importance of the wetting properties of the chemical solution.

While water is an excellent solvent for most metal nitrate precursors due to its high polarity, the aqueous solution exhibits inferior wetting properties on perovskite electrodes (e.g., LSCF) and fluoride electrolytes (e.g., GDC) due to the high surface tension of water ($72.0\ \text{mN m}^{-1}$ at 25°C) [11]. The surface tension of the aqueous solution can be reduced by adding organic solvents with low surface tension such as ethanol ($22.3\ \text{mN m}^{-1}$ at 25°C), acetone ($23.7\ \text{mN m}^{-1}$ at 25°C), and i-propanol ($21.7\ \text{mN m}^{-1}$ at 25°C). In this study, ethanol was chosen as a co-solvent considering the surface tension, miscibility with water and boiling temperature. The infiltration experiments using the porous LSCF–GDC electrode confirmed that the addition of ethanol to the aqueous solution remarkably improves the wetting characteristics. In particular, a solvent with the [water]/[ethanol] volume ratio of 1.7 was found to be adequate for balancing the capabilities of dissolving the nitrate precursors and penetrating into the submicron-scale pores. Fig. 2(c) shows the SSC nano-catalysts formed on the surface of the porous LSCF–GDC air electrode by infiltration of the chemical solution and *in-situ* crystallization at 800°C at the initial stage of the cell operation. The uniform dispersion of the primary particles across the entire air electrode as shown in Fig. 2(c) suggests the excellent wetting properties of the precursor solution on both LSCF and GDC because poor surface wetting would create the liquid beads, resulting in agglomerated particulate clusters [11]. In Fig. 3, SSC infiltration was performed with the precursor solution with the [water]/[ethanol] volume ratio of 3, and non-uniform distribution of the nano-particles is observed with severe agglomeration due to poor wetting properties. The diameter of the SSC nano-catalysts is within the range of $40\text{--}80\ \text{nm}$, and the homogeneous particle morphology and distribution clearly demonstrate the advantage of the urea decomposition technique in control of the nucleation process. In precipitation techniques, formation of deposit is initiated when the solubility limits of the metal cations are exceeded by the addition of the ligand into the precursor solution. Thus, the nucleation and growth kinetics of the precipitation techniques are controlled by the release rate of the ligand. Typically, the ligand is directly added to the solution, and the localized introduction of the ligand causes a rapid, non-uniform change of the solution concentration, resulting in irregular size and morphology of the synthesized particles. In contrast, in the urea decomposition process, urea is pre-mixed in the solution and slowly decomposes upon heating to $\sim 80^\circ\text{C}$, uniformly providing the ligand throughout the solution to initiate homogeneous precipitation. Thus, the kinetics of the nano-particle formation are well-controlled, resulting in excellent homogeneity in size and morphology of the nano-particles as

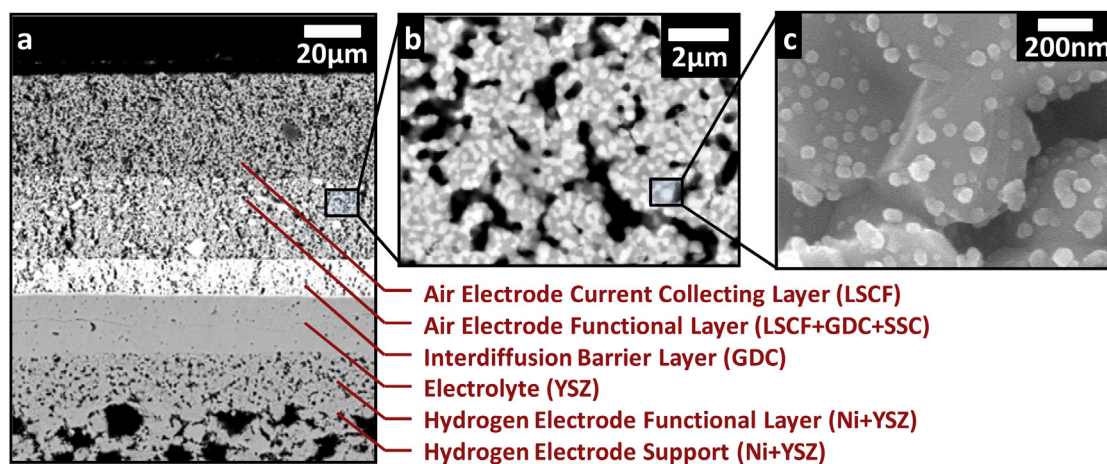


Fig. 2. SEM images of (a) the cross-section of the SORFC, (b) porous LSCF–GDC air electrode functional layer and (c) SSC nano-catalysts infiltrated into the LSCF–GDC air electrode.

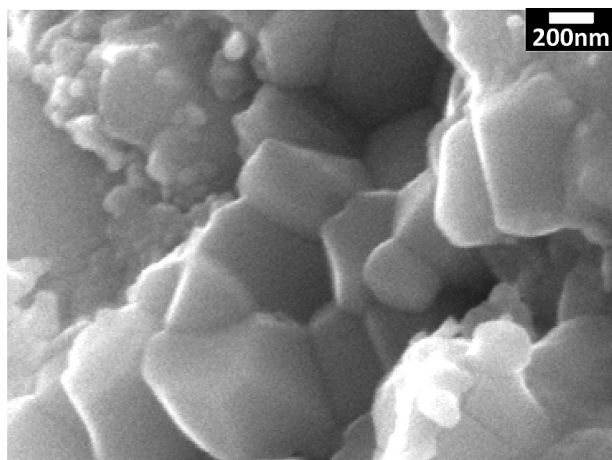


Fig. 3. SEM image of the air electrode infiltrated with the SSC precursor solution with the [water]/[ethanol] volume ratio of 3.

shown in Fig. 2(c). The uniform distribution of the nano-catalysts throughout the air electrode also suggests that precipitation occurred via homogeneous nucleation induced by urea decomposition rather than the evaporation of the solvent. If the formation of deposit is initiated by drying process rather than the urea decomposition, the capillary force brings the precursor solution to the surface of the porous matrix, resulting in an enrichment of the nano-particles near the top surface of the electrode [12]. In addition, considering that the SEM images in Fig. 2 were taken after the cell test for ~ 300 h, the absence of abnormal particle growth during that period of operation time in Fig. 2(c) implies the thermal stability of the SSC nano-catalysts against coarsening upon the SOFC operation at 700–800 °C.

The electrochemical performance of the cell infiltrated with the SSC nano-catalysts was evaluated, and its current density–voltage (I – V) curves and corresponding power densities are compared with those of the standard cell under the SOFC operation mode in Fig. 4(a). The measurements were performed at 750 °C with humidified H_2 (3% H_2O) as the fuel and air as the oxidant. The open circuit voltages (OCVs) of the two cells are very close to the theoretical value, showing that the electrolyte and sealing were leak-tight during testing. The maximum power density is 1.05 W cm^{-2} for the standard cell and 1.62 W cm^{-2} for the SSC-infiltrated cell. The power density at 0.7 V is 0.86 W cm^{-2} for the standard cell and 1.39 W cm^{-2} for the SSC-infiltrated cell. The results indicate that the performance can be improved by more than 60% under the practical SOFC operating conditions via the infiltration of the SSC nano-catalysts into the conventional LSCF–GDC air electrode. The same cells were also tested in both SOFC and SOEC modes at 750 °C with 50% H_2O in H_2 on the hydrogen electrode and air on the air electrode (Fig. 4(b)). The amount of steam supplied to the hydrogen electrode was fixed at 50% because we previously reported that this steam content is optimal for Ni–YSZ hydrogen electrode under the practical SOEC operation conditions considering both performance and stability; steam supply is insufficient at lower steam content, and higher steam content causes the local oxidation of Ni [16]. The measured OCVs of 0.96 V for both cells are in excellent agreement with the theoretical value for the given operating condition, indicating that the intended amount of steam was properly supplied to the hydrogen electrode. The SSC-infiltrated cell shows a significantly shallower slope in the I – V curve than the standard cell in both SOFC and SOEC modes, indicating the reduced cell resistance due to the SSC infiltration. In SOEC mode, the hydrogen production rate at thermal neutral voltage is important because the

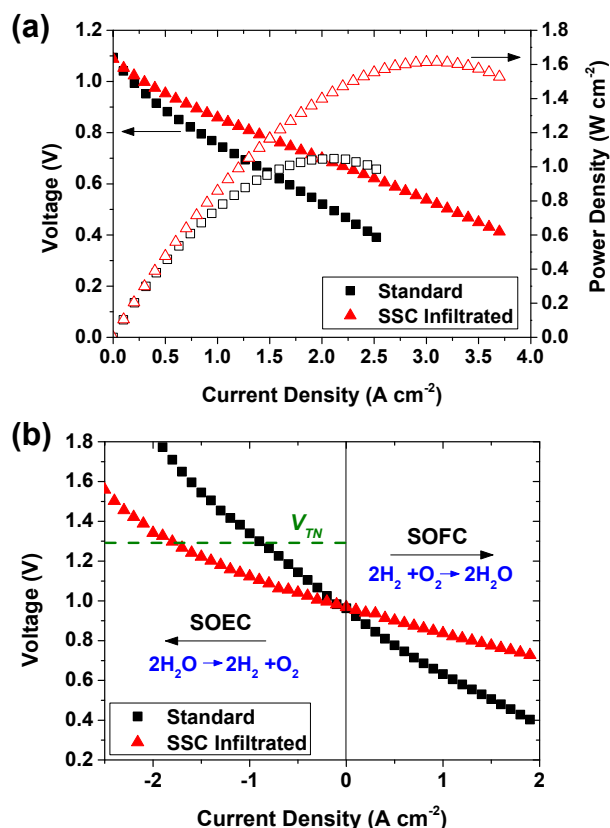


Fig. 4. (a) I – V curves and corresponding power densities of the standard and SSC-infiltrated cells measured in SOFC mode at 750 °C with humidified hydrogen (3% H_2O) on a hydrogen electrode and air on air electrode, and (b) I – V curves of the standard and SSC-infiltrated cells measured in SOFC and SOEC modes at 750 °C with humidified hydrogen (50% H_2O) on a hydrogen electrode and an air on air electrode. V_{TN} represents thermal neutral voltage for steam decomposition.

endothermic heat of steam decomposition is compensated by ohmic heating and the reaction for hydrogen production can be sustained without an external heat source above that potential [17]. The thermal neutral voltage is 1.29 V at 750 °C [18], at which the current density is increased from 0.9 to 1.8 A cm^{-2} by infiltration of the SSC nano-catalysts, which corresponds to the doubling of the H_2 production rate from 3.7 to $7.4 \text{ Nm}^3 \text{ m}^{-2} \text{ h}^{-1}$ under the practical SOEC operating conditions.

In Fig. 5, the effect of the SSC infiltration on the performance of the SOFC is systematically analyzed using impedance spectroscopy performed under various operating conditions. In the Nyquist plot of the impedance spectra, the high-frequency intercept corresponds to the ohmic resistance of the cell, and the low-frequency intercept represents the total cell resistance including the ohmic resistance and electrode polarization resistance. Therefore, the electrode polarization resistance can be obtained by subtracting the high-frequency intercept from the low-frequency intercept [19]. The impedance spectra measured at OCV in Fig. 5(a) show that SSC infiltration slightly lowers the ohmic resistance and remarkably reduces the electrode polarization resistance. It is considered that the slight decrease in the ohmic resistance with SSC infiltration results from the local network of the SSC nano-particles formed on the surface of the LSCF–GDC electrode, which provides additional conduction paths for electric current, because the electrical conductivity of SSC ($> 1000 \text{ S cm}^{-1}$ at 800 °C [8]) is substantially higher than that of LSCF ($\sim 300 \text{ S cm}^{-1}$ at 800 °C [20]). To explain the drastic reduction of the electrode polarization resistance due to the

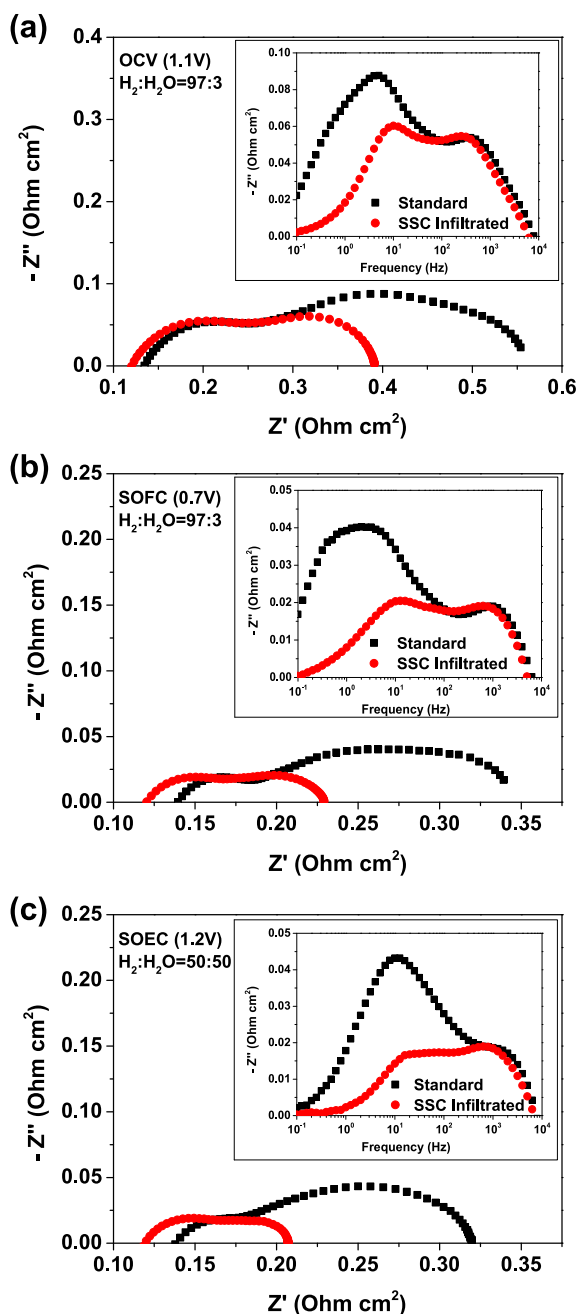


Fig. 5. Impedance spectra of the standard and SSC-infiltrated cells measured at 750 °C with (a) humidified hydrogen (3% H_2O) on a hydrogen electrode and an air on air electrode at the OCV, (b) humidified hydrogen (3% H_2O) on a hydrogen electrode and air on an air electrode at 0.7 V in SOFC mode, and (c) humidified hydrogen (50% H_2O) on a hydrogen electrode and air on an air electrode at 1.2 V in SOEC mode.

SSC infiltration, it is necessary to understand the electrode reaction kinetics and elementary reaction pathways associated with the frequency response of the impedance spectra. It is known that the impedance spectra of the air electrode are composed of a number of overlapping depressed arcs, reflecting physical and/or chemical processes associated with the electrode reaction [21]. Individual elementary processes exhibit their unique characteristic frequencies and different responses to the modification of the electrode materials and structure. The Bode plot in the insert of Fig. 5(a) clearly shows that the impedance spectra of the tested cells are composed of two dominant arcs with characteristic frequencies of

10^2 – 10^3 Hz and 1–10 Hz. The size of the low-frequency arc (1–10 Hz) is significantly reduced by SSC infiltration while the high-frequency arc (10^2 – 10^3 Hz) is relatively insensitive to the modification of the air electrode. Similar trends are consistently observed under the both SOFC (0.7 V) and SOEC (1.2 V) operating conditions in Fig. 5(b) and (c), respectively. Recently, we have analyzed the impedance spectra of the air/hydrogen electrodes separately using the half cell techniques and successfully correlated the results with the full cell data [5,16]. It was found that the performance of the LSCF–GDC air electrode is governed by a low-frequency impedance (1–10 Hz), which is associated with surface chemical exchange, while a small contribution of the ionic diffusion of oxygen appears at a higher frequency range (10^2 – 10^3 Hz) [5]. In case of the Ni–YSZ hydrogen electrode, the major impedance arc is generated by gas–solid interactions at 10^2 – 10^3 Hz, and gas phase diffusion across the thick substrate can produce a low-frequency impedance arc (1–10 Hz) for the hydrogen electrode-supported configuration [22]. These findings can be directly applied to the interpretation of the full cell impedance. In particular, the high-frequency arc (10^2 – 10^3 Hz) in Fig. 5 is dominated by the gas–solid interaction at the Ni–YSZ hydrogen electrode because the contributions of the ionic diffusion of oxygen at the LSCF–GDC air electrode is relatively small [5], and the low-frequency arc (1–10 Hz) contains the contributions of both the surface chemical exchange at the LSCF–GDC air electrode and gas diffusion across the Ni–YSZ hydrogen electrode substrate. Thus, the surface chemical exchange is suggested to be the governing reaction for the LSCF–GDC air electrode, which is consistent with previous observations [23], implying that incorporation of the SSC nano-catalysts can effectively improve the electrode performance via acceleration of the rate limiting process and suppression of the low-frequency impedance arc as shown in Fig. 5(a)–(c). At the air electrode, oxygen reduction occurs in power generation mode, and oxygen gas evolution occurs in hydrogen production mode. Thus, it is concluded that the surface chemical exchange for both O_2 reduction (Fig. 5(b)) and O_2^{2-} oxidation (Fig. 5(c)) can be remarkably accelerated by the incorporation of SSC nano-catalysts in the porous LSCF–GDC air electrode, resulting in a substantial improvement of SOFC and SOEC performance. In this approach, the major benefits of SSC and LSCF–GDC in catalytic activity and stability, respectively, can be utilized simultaneously. In addition, the infiltration technique developed in this study can be readily implemented in large-scale production via well-developed and cost-effective solution injection techniques, eventually facilitating the successful development and deployment of SORFC technology.

4. Conclusions

Although SSC is an excellent catalyst and electrode material, its practical application has been limited, mainly due to its lack of thermal compatibility with other cell components. In this study, these inherent limitations are successfully overcome by incorporating SSC nano-catalysts into the conventional LSCF–GDC air electrode scaffold. An infiltration and *in-situ* crystallization technique based on the urea decomposition process is developed to synthesize SSC nano-catalysts, and the uniform distribution of extremely fine SSC catalysts is achieved by homogeneous nucleation. The remarkable enhancement of the surface chemical exchange rate is confirmed by impedance analysis, resulting in a significant improvement in electrochemical performance in both SOFC and SOEC modes. Further improvement is expected through the optimization of materials and processing parameters, and eventually, the technique developed in this study is expected to contribute to the successful commercialization of SORFC technology.

Acknowledgments

This research was financially supported by the institutional research program of the Korea Institute of Science and Technology (2E24042) and the Fundamental Research and Development Program for Core Technology of Materials, funded by the Ministry of Knowledge Economy, Republic of Korea.

References

- [1] G.-B. Jung, J.-Y. Chen, C.-Y. Lin, S.-Y. Sun, *Int. J. Hydrogen Energy* 37 (2012) 15801–15807.
- [2] M.A. Laguna-Bercero, R. Campana, A. Larrea, J.A. Kilner, V.M. Orera, *Fuel Cells* 11 (2011) 116–123.
- [3] M.A. Laguna-Bercero, *J. Power Sources* 203 (2012) 4–16.
- [4] K.J. Yoon, S. Gopalan, U.B. Pal, *J. Electrochem. Soc.* 156 (2009) B311–B317.
- [5] J. Kim, D. Shin, J.-W. Son, J.-H. Lee, B.-K. Kim, H.-J. Je, H.-W. Lee, K.J. Yoon, *J. Power Sources* 241 (2013) 440–448.
- [6] H. Fukunaga, M. Koyama, N. Takahashi, C. Wen, K. Yamada, *Solid State Ionics* 132 (2000) 279–285.
- [7] F.S. Baumann, J. Fleig, G. Cristiani, B. Stuhlhofer, H.-U. Habermeier, J. Maier, *J. Electrochem. Soc.* 154 (2007) B931–B941.
- [8] T. Ishihara, M. Honda, T. Shibayama, H. Minami, H. Nishiguchi, Y. Takita, *J. Electrochem. Soc.* 145 (1998) 3177–3183.
- [9] H. Lv, Y.-j. Wu, B. Huang, B.-y. Zhao, K.-a. Hu, *Solid State Ionics* 177 (2006) 901–906.
- [10] H.Y. Tu, Y. Takeda, N. Imanishi, O. Yamamoto, *Solid State Ionics* 100 (1997) 283–288.
- [11] X. Lou, S. Wang, Z. Liu, L. Yang, M. Liu, *Solid State Ionics* 180 (2009) 1285–1289.
- [12] S. Jung, C. Lu, H. He, K. Ahn, R.J. Gorte, J.M. Vohs, *J. Power Sources* 154 (2006) 42–50.
- [13] H.Y. Jung, S.H. Choi, H. Kim, J.W. Son, J. Kim, H.W. Lee, J.H. Lee, *J. Power Sources* 159 (2006) 478–483.
- [14] D. Sordellet, M. Akinc, *J. Colloid Interface Sci.* 122 (1988) 47–59.
- [15] G.J.d.A.A. Soler-Illia, R.J. Candal, A.E. Regazzoni, M.A. Blesa, *Chem. Mater.* 9 (1997) 184–191.
- [16] H.P. Dasari, S.-Y. Park, J. Kim, J.-H. Lee, B.-K. Kim, H.-J. Je, H.-W. Lee, K.J. Yoon, *J. Power Sources* 240 (2013) 721–728.
- [17] W. Doenitz, R. Schmidberger, *Int. J. Hydrogen Energy* 7 (1982) 321–330.
- [18] O.A. Marina, L.R. Pederson, M.C. Williams, G.W. Coffey, K.D. Meinhardt, C.D. Nguyen, E.C. Thomsen, *J. Electrochem. Soc.* 154 (2007) B452–B459.
- [19] J.E. Bauerle, *J. Phys. Chem. Solids* 30 (1969) 2657–2670.
- [20] A. Petric, P. Huang, F. Tietz, *Solid State Ionics* 135 (2000) 719–725.
- [21] S.H. Jensen, A. Hauch, P.V. Hendriksen, M. Mogensen, N. Bonanos, T. Jacobsen, *J. Electrochem. Soc.* 154 (2007) B1325–B1330.
- [22] Y.-G. Choi, J.-Y. Park, H. Song, H.-R. Kim, J.-W. Son, J.-H. Lee, H.-J. Je, B.-K. Kim, H.-W. Lee, K.J. Yoon, *Ceram. Int.* 39 (2013) 4713–4718.
- [23] E.N. Armstrong, K.L. Duncan, D.J. Oh, J.F. Weaver, E.D. Wachsman, *J. Electrochem. Soc.* 158 (2011) B492–B499.